Electronic Supplementary Material (ESI) for Journal of Materials Chemistry A.

Supporting Information

Molten Salt- Directed Synthesis of Strontium Manganese Perovskite Oxide: An Active Electrocatalyst for Oxygen Reduction Reaction and Oxygen Evolution Reaction

Carolin Mercy Enoch,[a] Sagar Ingavale,[a] Phiralang Marbaniang,[a] Indrajit Patil,[b] and Anita Swami[a]*

[a] Department of Chemistry,[a] SRM Institute of Science and Technology, Kattankulathur-603203,Chennai, India

[b] Department of Physics and Centre for Energy Science, Indian Institute of Science Education and Research (IISER) Pune, Maharashtra - 411008, India

*Corresponding author e-mail: swamians@srmist.edu.in, swami.anita@gmail.com

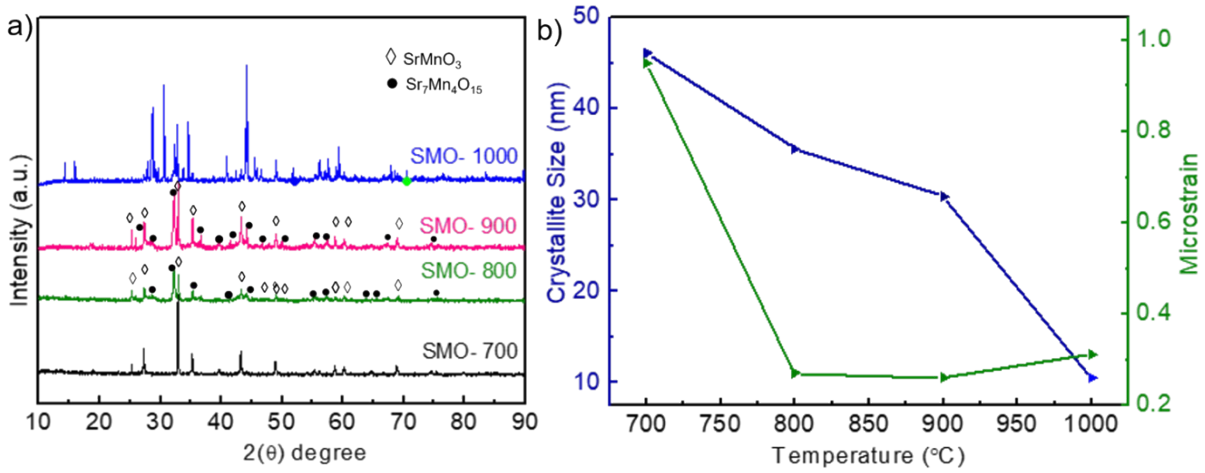

Figure S1. (a) XRD patterns of strontium manganese perovskite oxides; (b) Crystallite size calculated using Debye-Scherrer formula and microstrain plotted as a function of temperature.

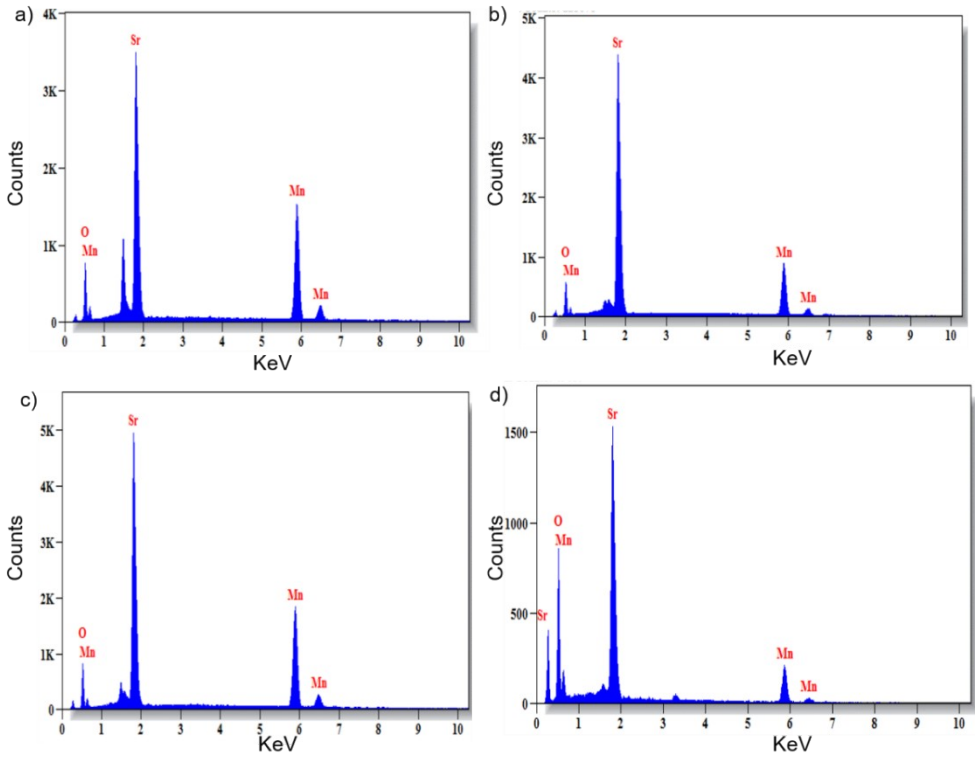

Figure S2. EDS profiles of (a) SMO-700; (b) SMO-800; (c) SMO-900; and (d) SMO-1000.

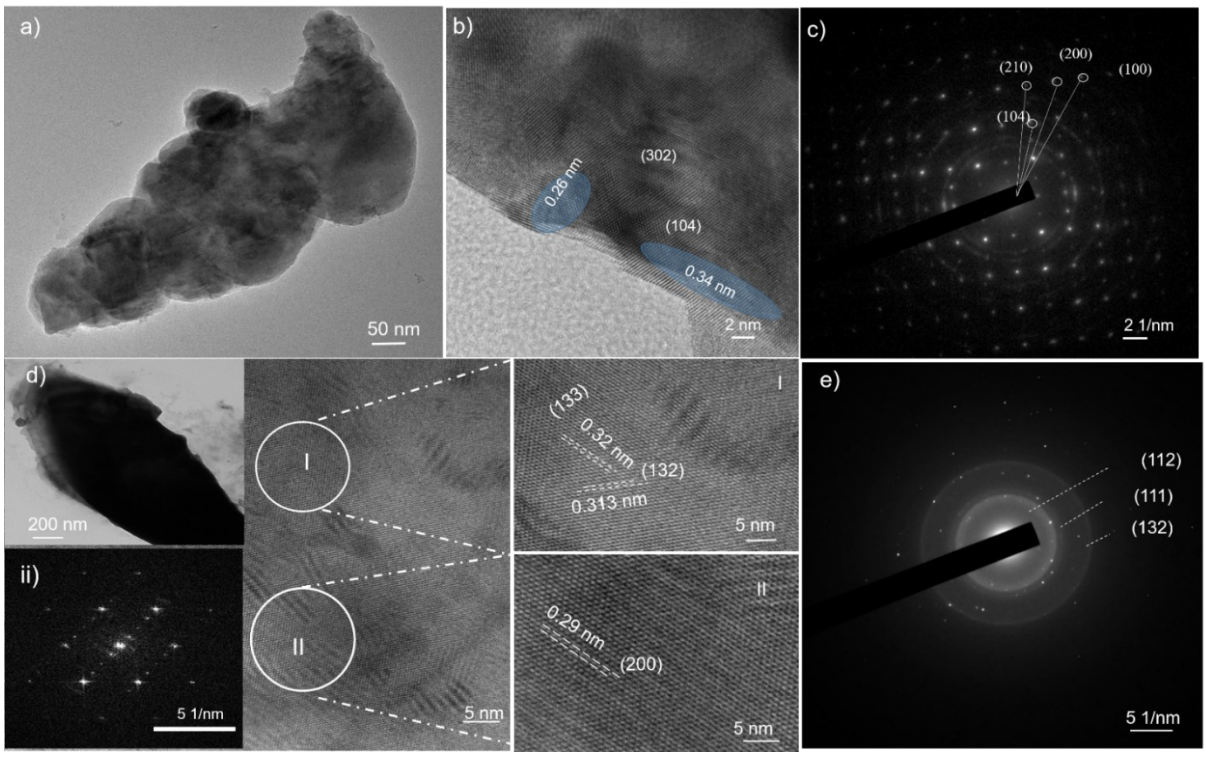

Figure S3. (a) TEM image and (b) HRTEM image showing lattice fringes corresponding to (302), (104) of SMO-700 ($SrMnO_3$); (c) SAED pattern of SMO-700; (d) HRTEM image (corresponding TEM image and FFT in insets) of SMO-1000; whereas zoom images (I and II) show the lattice planes corresponding to (133) (132) and (200); and (e) SAED pattern of SMO-1000.

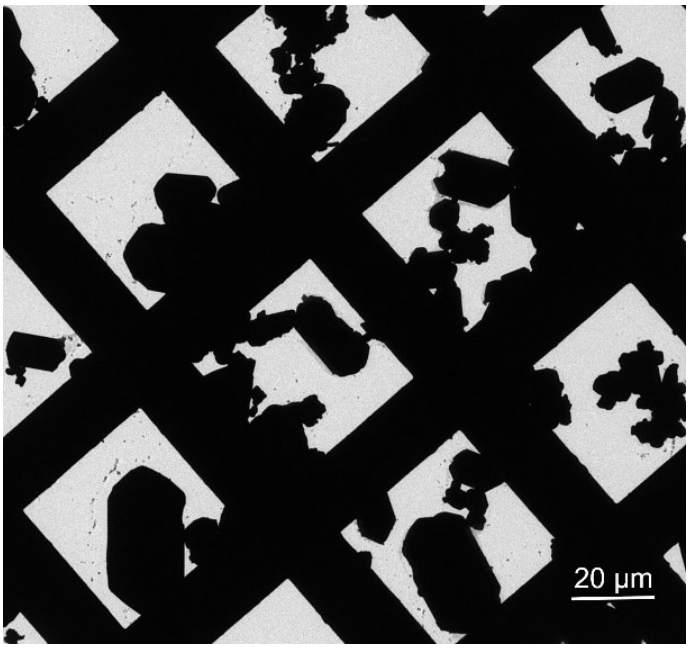

Figure S4. TEM image of SMO-1000.

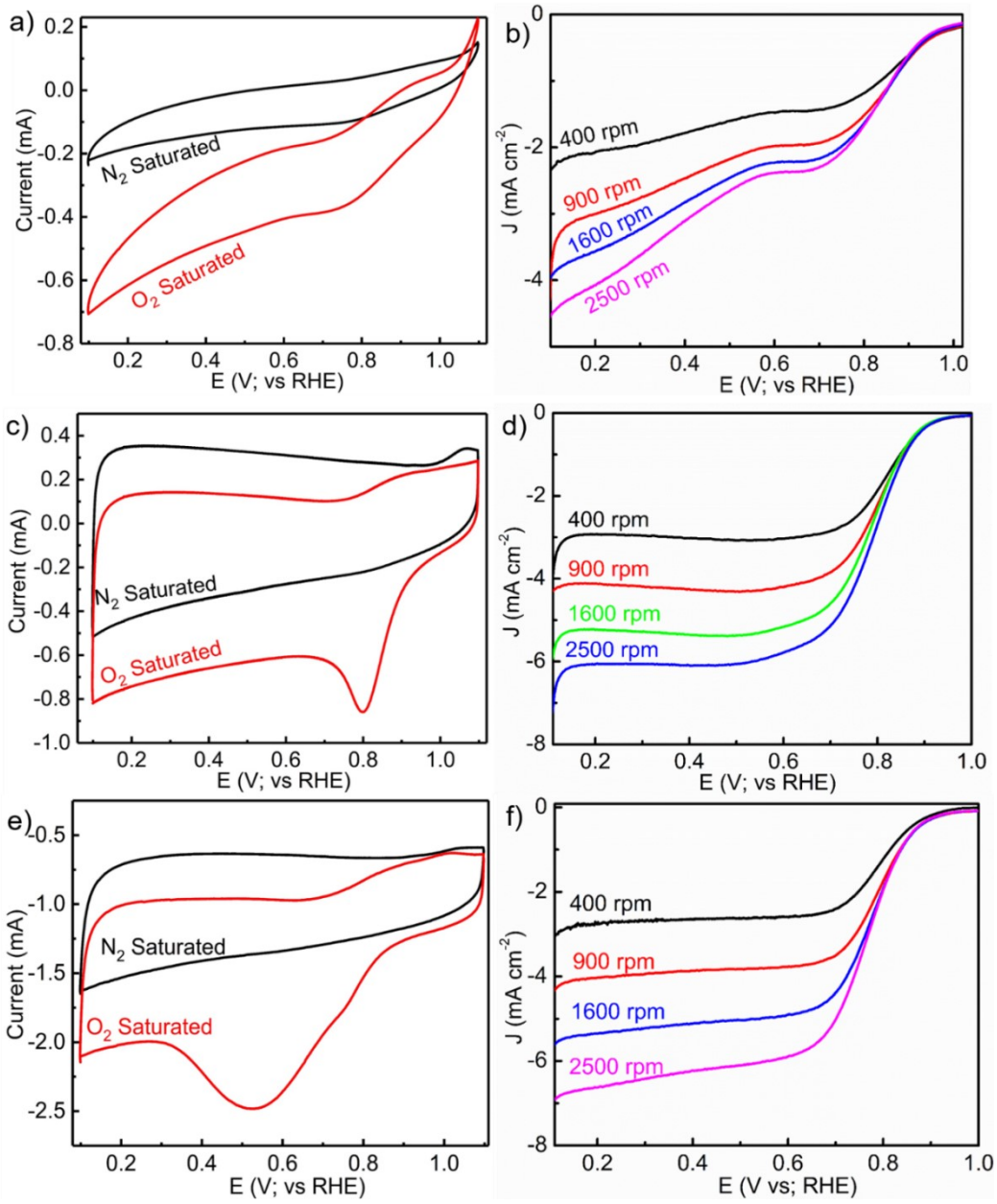

Figure S5. Comparative CVs in N_2 and O_2 saturated 0.1 M KOH solution at scan rate 20 mV s^{-1} of (a) SMO-700; (c) SMO-800; (e) SMO-1000; and corresponding ORR polarization curves at different rotation rates in O_2 saturated 0.1 M KOH for (b) SMO-700; (d) SMO-800; and (f) SMO-1000.

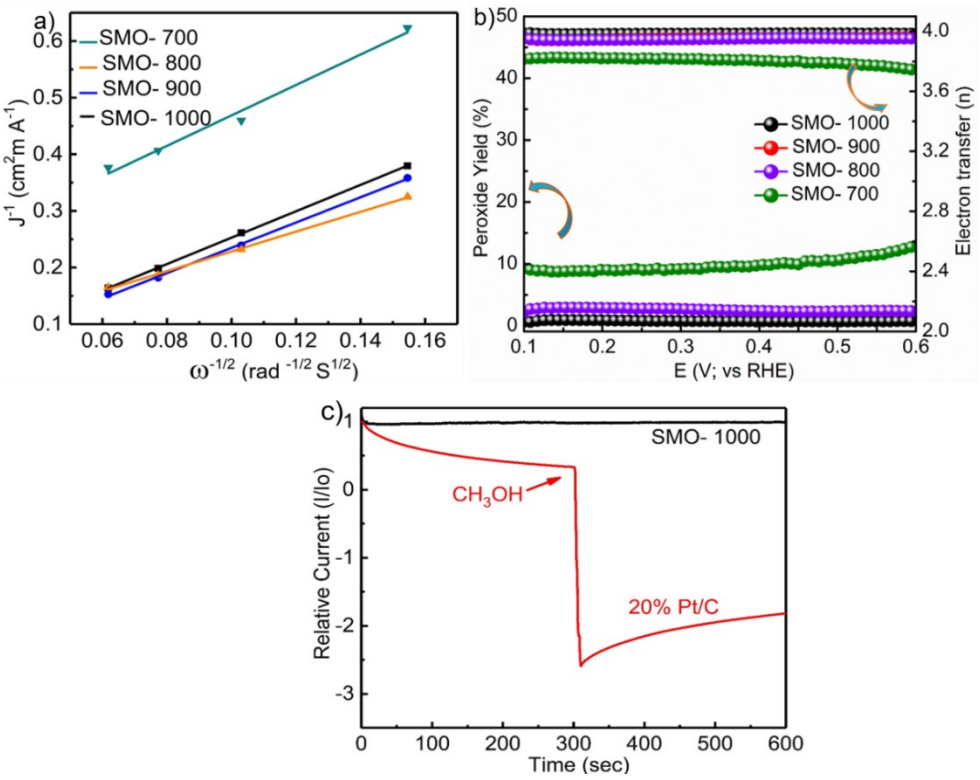

Figure S6. (a) Koutecky-Levich plots obtained at 0.5 V vs. RHE from figure 6 (a); (b) RRDE measurements of all the catalysts showing the percentage of peroxide and electron transfer number; (c) Chronoamperometric responses (current versus time) of SMO-1000 and Pt/C catalyst before and after addition of 1 M methanol recorded at fixed potential.

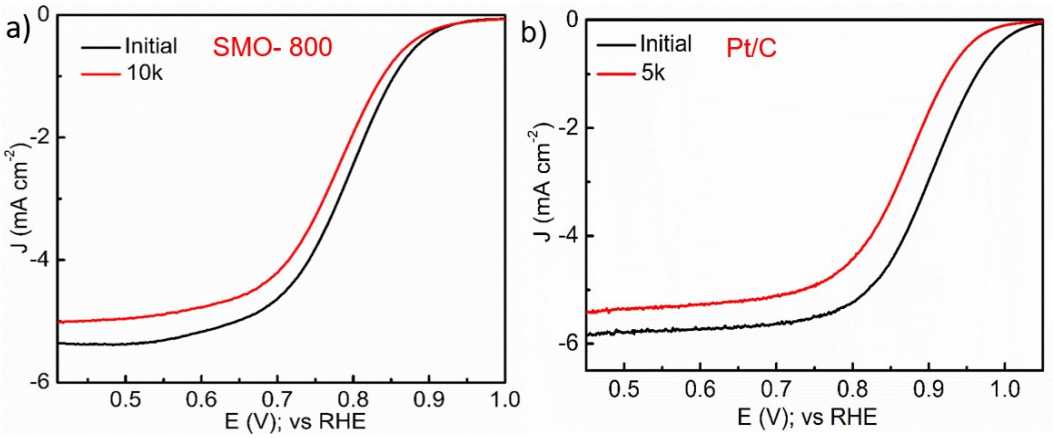

Figure S7. ORR polarization curves of (a) SMO-800; and (b) commercial Pt/C catalyst recorded initially and after 10k and 5k cycles respectively.

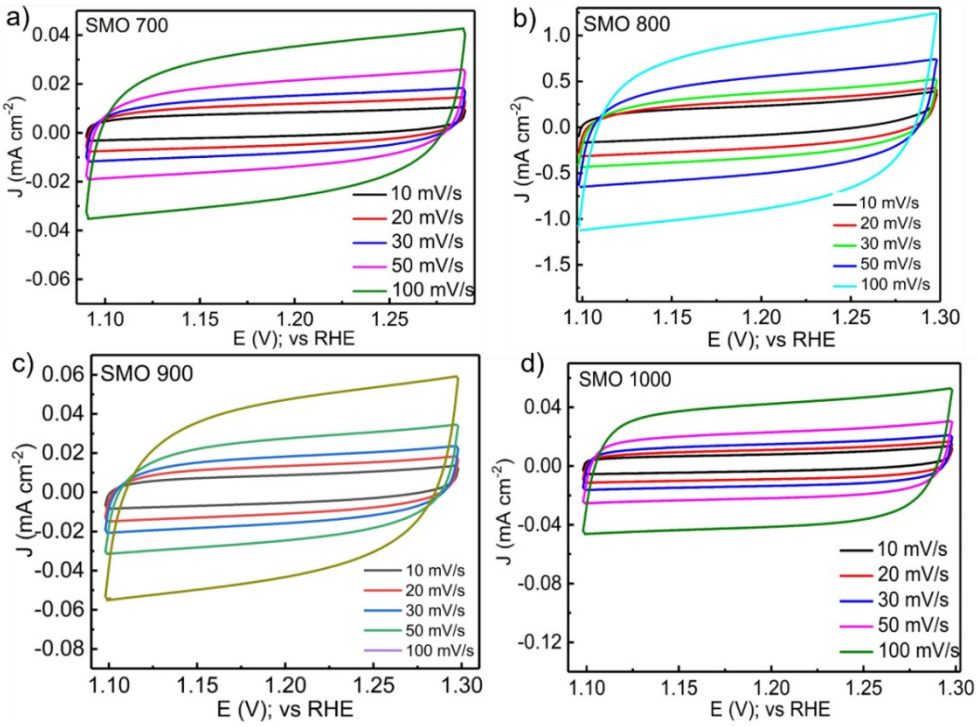

Figure S8. Cyclic voltammograms recorded in non-faradaic region for all the catalysts.

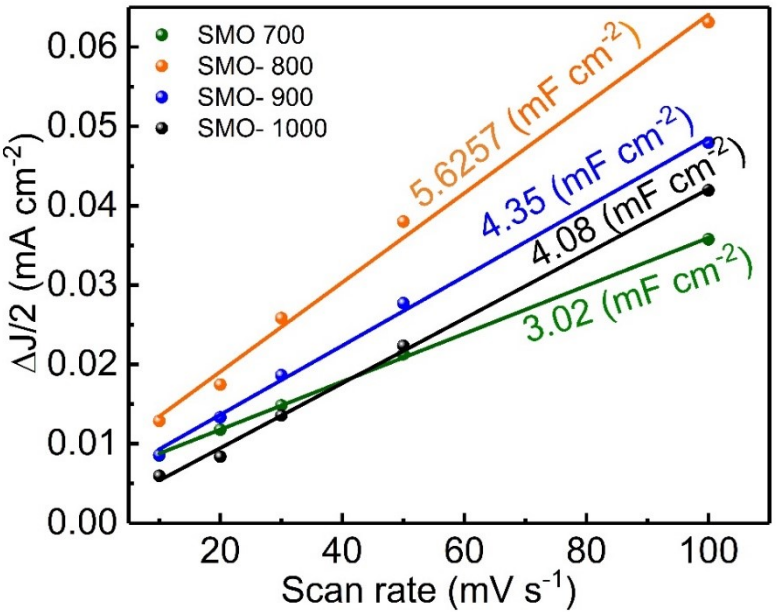

Figure S9. Current densities ($J = J_{anode} - J_{cathode}$) as a function of scan rate for SMO-700, SMO-800, SMO-900 and SMO-1000 with the slope proporational to C_{dl} values.

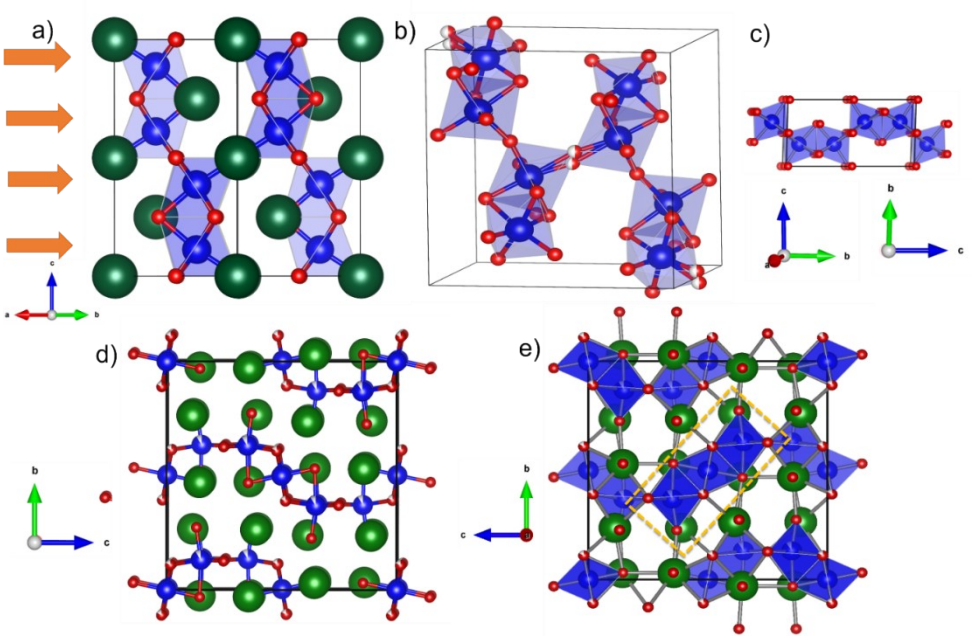

Figure S10. (a) Crystal structures of 4-H $SrMnO_3$ stacking layers; (b-c) Crystal structures of SMO-900 Phase-I ($Sr_7Mn_4O_{15}$) and Phase-II ($SrMnO_3$); (d) Crystal structure of SMO-1000 showing zig-zag layers of Mn-O linkages; and (e) $Sr_4Mn_3O_{10}$ describing Mn_3O_{10} units. In all figures green ball represents strontium, blue ball represents manganese and red ball represents oxygen.

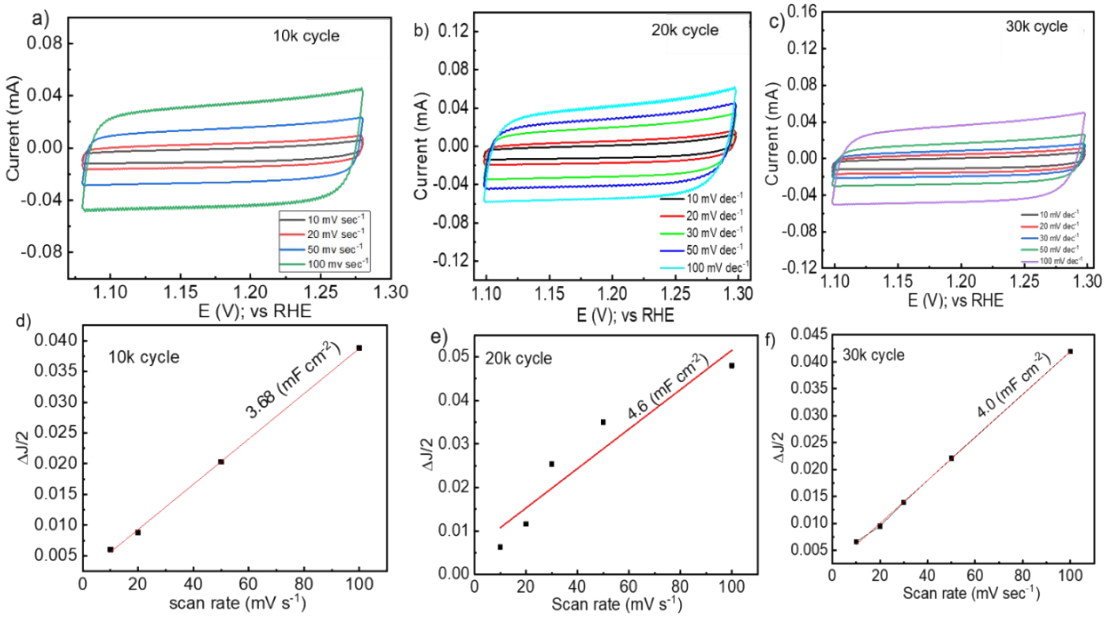

Figure S11. (a-c) Cyclic voltammograms recorded at different time intervals during the stability test (10k, 20k and 30k cycles) for SMO-1000 catalyst; and (d-f) corresponding current densities ($J= J_{anode}- J_{cathode}$) as a function of scan rate.

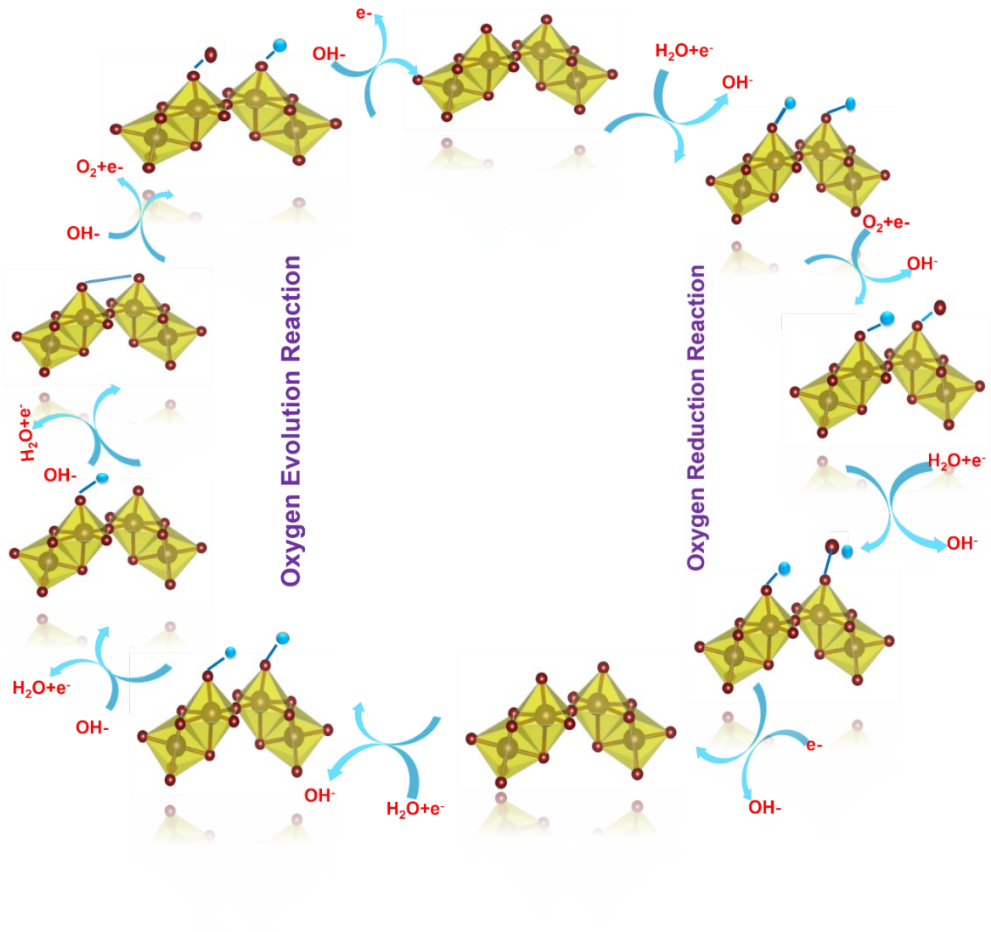

Figure S12. A proposed bi-functional mechanism for $Sr_4Mn_3O_{10}$ catalytic surface. The navy blue ball inside the polyhedra represents manganese, the brown ball represents oxygen, and the blue ball represents hydride.

Table S1. Summary of refined cell parameters of SMO-700, SMO-800, SMO-900and SMO-1000.

Catalyst	Lattice parameter (Å)			Crystal System	Space group & Space number	Rwp(%)	Rp(%)	Volume Fraction (%)
	a	b	c					
SMO- 700 $SrMnO_3$	5.4484	5.4484	9.0865	Hexagonal	P 63/mmc &194	48.5	77.9	100
SMO- 800 $SrMnO_3$/$Sr_7Mn_4O_{15}$	5.4484 6.8472	5.4484 9.6585	9.0865 10.2749	Hexagonal/ Monoclinic	P 63/mmc& 194 P1 21/c1 & 14	51.3	63.1	11.6 88.4
SMO- 900 $SrMnO_3$/ $Sr_7Mn_4O_{15}$	5.4507 6.8355	5.4507 9.6364	9.0900 10.3544	Hexagonal/ Monoclinic	P 63/mmc& 194 P1 21/c1 & 14	45.8	54.2	28.19 71.8
$Sr_4Mn_3O_{10}$	5.4770	12.4625	12.5349	Orthorhombic	Cmca& 64	56.4	42.9	100

R_{wp} Residual weight parameter, R_p Residual parameter

Table S2. Reflection planes of **(**a) SMO-700; (b) SMO-800; (c) SMO-900; and (d) SMO-1000.

a)

No.	2 θ	hkl
1	18.7798	100
2	19.511	002
3	21.1868	101
4	27.2095	102
5	32.8294	110
6	35.1585	103
7	38.0892	200
8	38.4763	112
9	39.4034	201
10	39.6182	004
11	43.1447	202
12	44.1866	104
13	48.8638	203
14	51.1459	210
15	52.1944	211
16	52.3672	114
17	53.9938	105
18	55.2556	212
19	56.1265	204
20	58.6097	300
21	59.5684	301
22	60.123	213
23	61.1055	006
24	62.3905	302
25	64.5349	106
26	64.6491	205
27	66.5687	214
28	66.9419	303
29	68.829	220
30	71.1261	116
31	72.0663	310
32	72.3182	222

b)

No.	Code (Phases)	2 θ	hkl
1	1	25.2976	022
2	2	25.3615	022
3	1	26.0234	200
4	2	26.0892	200
5	2	30.7476	130
6	2	30.7852	-202
7	1	37.4481	-213
8	2	37.5447	-213
9	1	37.9551	104
10	1	37.9906	-114
11	2	45.185	204
12	2	45.2044	015
13	2	45.2499	034
14	2	45.2806	-123
15	1	46.4955	-115
16	2	46.6179	-115
17	1	47.1039	241
18	1	47.151	-242
19	2	48.0122	051
20	1	48.0974	025
21	1	51.5658	-332
22	2	53.0497	332
23	1	53.2956	-314
24	2	53.4386	-314
25	2	65.0798	226
26	1	67.059	404

c)

No.	Code (Phases)	2 θ	hkl
1	1	12.9335	100
2	2	12.9658	100
3	1	15.8649	110
4	2	15.9046	110
5	1	18.3727	111
6	2	18.4188	111
7	1	26.0356	200
8	2	26.1015	200
9	1	27.64	013
10	1	30.0762	-113
11	2	30.1528	-113
12	2	32.1674	131
13	1	34.1883	-123
14	2	34.2759	-123
15	1	36.1947	014
16	2	36.2879	014
17	1	38.0102	104
18	2	38.0889	-114
19	1	39.1045	-231
20	2	39.2057	-231
21	1	46.1633	214
22	2	46.2847	214
23	1	55.1092	304
24	2	55.2579	304
25	1	55.9407	-153
26	2	56.0921	-153

d)

No.	2 θ	hkl
1	14.119	002
2	14.202	020
3	15.87	021
4	19.048	111
5	20.078	022
6	25.649	023
7	26.0356	200
8	28.459	004
9	28.628	040
10	31.94	024
11	32.055	042
12	35.752	202
13	35.787	220
14	40.807	044
15	55.259	206
16	55.479	260
17	58.893	008
18	68.466	400
19	70.316	402
20	75.7457	404
21	75.83	440

Table S3. Oxygen and manganese contents for SMO-900 ($Sr_7Mn_4O_{15}/SrMnO_3$) and SMO-1000 ($Sr_4Mn_3O_{10}$) obtained from XPS.

Composition (%)	Mn^{4+}	Mn^{3+}	O species			
			$O_{surface}$		$O_{Lattice}$	
			O_{ad}	M-O		
SMO-900 ($Sr_7Mn_4O_{15}$/ $SrMnO_3$)	27%	73%	31.4%	32.4%	36.2%	
SMO-1000 ($Sr_4Mn_3O_{10}$)	34%	66%	57.7%		19.1%	23.2%

Table S4. Summary of electrochemical data (onset and half-wave potential, limiting currrent density and the number of electrons transferred) for all the synthesized catalysts.

Electrocatalyst	**E_{onset} (V; vs. RHE)**	**$E_{1/2}$ (V)**	**J_L @0.2 V (mA cm^{-2})**	**'*n*' from RRDE**
SMO-700 $SrMnO_3$	0.96	0.82	3.57	3.7
SMO-800 $SrMnO_3/Sr_7Mn_4O_{15}$	0.93	0.79	5.24	3.95
SMO-900 $SrMnO_3/Sr_7Mn_4O_{15}$	0.97	0.82	5.56	3.98
SMO-1000 $Sr_4Mn_3O_{10}$	0.91	0.78	5.34	4.0
Pt/C	0.99	0.9	5.85	4.0

Table S5. O1-O1 bond distance in (Å) and O– Mn–O bond angles (°) as observed in SMO-700, SMO-800, SMO-900 and SMO-1000.

Catalyst	Composition	O1-O1 (Å)	O-Mn-O (°) Face sharing	O-Mn-O (°) Corner sharing
SMO-700	$SrMnO_3$	2.7483	93.3831	171.47
SMO-800	$Sr_7Mn_4O_{15}$	2.0371	93.5364	177.45
	$SrMnO_3$	3.10359	73.3090	173.269
SMO-900	$Sr_7Mn_4O_{15}$	2.0493	93.5735	175.49
	$SrMnO_3$	3.10394	79.3681	173.184
SMO-1000	$Sr_4Mn_3O_{10}$	2.77243	89.75	180

Table S6. Bond lengths of Mn-O (1) (Å) / Mn-O (2) (Å)/ Mn-O(1)-Mn(Å)/Mn-O(2)-Mn(Å)/Mn-Mn(Å) as observed in SMO-700, SMO-800, SMO-900 and SMO-1000.

Catalyst	Composition	Mn-O(1) (Å)	Mn-O(2) (Å)	Mn-O(1)-Mn (Å)	Mn-O(2)-Mn (Å)	Mn-Mn (Å)
SMO-700	$SrMnO_3$	1.8716	1.9013	2.73	1.8116	2.532
SMO-800	$Sr_7Mn_4O_{15}$	1.8965	2.06081	1.8764	1.7430	2.5328
	$SrMnO_3$	2.32566	2.31212	2.31212/ 79.54	2.31212	2.83262
SMO-900	$Sr_7Mn_4O_{15}$	1.8025	2.06349	1.8974	1.7430	2.54318
	$SrMnO_3$	(Mn2)-(O3): 2.31650	(Mn2) -(O5): 2.31301	76.8491/ 2.31	32.3407/ 2.31650	2.86689
SMO-1000	$Sr_4Mn_3O_{10}$	1.925	2.024	1.92568	-	2.483

Table S7. ECSA, mass activity and specific activity listed for all the synthesized catalysts.

Electrocatalyst	**ECSA (m^2/g))**	**Mass Activity ($mA\ mg^{-1}$)**	**Specific Activity ($mA\ cm^{-2}$)**
SMO-700 $SrMnO_3$	1.33	9.7	0.73
SMO-800 $SrMnO_3/Sr_7Mn_4O_{15}$	2.48	66.6	2.63
SMO-900 $SrMnO_3/Sr_7Mn_4O_{15}$	1.92	126.8	6.61
SMO-1000 $Sr_4Mn_3O_{10}$	1.2	41.5	3.46

Table S8. Summary of the literature reports for ORR and OER performance.

Electrocatalyst	**Catalyst loading** (mg cm^{-2})	**E_{onset} (V; vs RHE)**	**Current density at 0.7 V (mA cm^{-2})**	**$E_{1/2\ (ORR)}$ (V; vs RHE)**	**$E_{j\text{-}10\ (OER)}$ (V; vs RHE)**	**$E_{j\text{-}10(OER)}$-$E_{1/2(ORR)}$ (V; vs RHE)**	**Ref.**
SMO- 700 $SrMnO_3$	0.566	0.96	2.16	0.82	-	-	This work
SMO-800 $SrMnO_3/Sr_7Mn_4O_{15}$ (11.6% and 88.4%)	0.566	0.93	4.6	0.79	-	-	This work
SMO-900 $SrMnO_3/Sr_7Mn_4O_{15}$ (36.9% & 66.06%)	0.566	0.97	5.16	0.82	1.93	1.11	This work
SMO- 1000 $Sr_4Mn_3O_{10}$	0.566	0.91	4.35	0.78	1.72	0.94	This Work
$LaMnO_3$	0.312	-	-	0.67	1.80	1.13	1
$LaMn_{0.4}Co_{0.6}O_3$	0.312	-	-	0.71	1.63	0.92	1
$LaMn_{0.2}Co_{0.8}O_3$	0.312	-	-	0.68	1.64	0.96	1
$La_{0.4}Sr_{0.6}MnO_3$	0.5	-0.197 vs SCE (V)	4.54	-	0.774 @ 5 mA cm^{-2}	0.97	2
$La_{0.8}Sr_{0.2}Mn_{1-x}Ni_xO_3$	NA	0.74	-	-	1.54 @ 2mA cm^{-2}	-	3
$La_{23}/Sr_{1/3}MnO_3$	0.5	0.87	-	0.8	-	-	4
$MnO_2/La_{0.7}Sr_{0.3}MnO_3$	0.47	0.87	-	0.75	1.727	0.89	5
$Sr_4Mn_3O_{10}$	NA	0.80	-	0.5	-	-	6
$La_{0.9}Y_{0.1}MnO_3$	0.236	0.90	6.58	0.75	1.8	-	7
$LKMnO_3$		-	-	0.78	1.66	-	8
$La_{0.6}Ca_{0.4}CoO_3$/Sb doped SnO_2	NA	0.76	2.8	0.79	1.60	-	9
$A_xSm_{1-x}Mn_2O_{5-\delta}(Ba_xSn_{1-x}Mn_2O_{5-\delta})$	0.25	0.884		0.789			10
$La_{0.85}Y_{0.15}Ni_{0.7}Fe_{0.3}O_3$	0.2	0.71	3.7	0.62	1.63 @ 10 mA		11
$La_2Co_{0.5}Fe_{0.5}MnO_{6-\delta}$	NA	0.78	6.1	0.62	1.65		12
$LaCoO_3$ @ rGO	NA	0.85	5.5	0.70	1.51		13
$La_{0.8}Sr_{0.2}Ti_{0.65}\ Fe_{0.35}O_{3-\delta}$ LSTFO/NCNT	1.0	0.992	6.07	0.86	1.77	0.76	14

NA- Not Available

References

1. Jiang, X., Dong, Y., Zhang, Z., Li, J., Qian, J., & Gao, D.. Cation substitution of B-site in $LaCoO_3$ for bifunctional oxygen electrocatalytic activities. *Journal of Alloys and Compounds*, **2021**, 878, 160433.

2. Zhao, Y., Hang, Y., Zhang, Y., Wang, Z., Yao, Y., He, X., ... & Zhang, D.). Strontium-doped perovskite oxide $La_{1-x}Sr_xMnO_3$ (x= 0, 0.2, 0.6) as a highly efficient electrocatalyst for nonaqueous Li-O_2 batteries. *Electrochimica Acta*,**2017**, 232, 296-302.

3. Islam, M., Jeong, M. G., Oh, I. H., Nam, K. W., & Jung, H. G. (2020). Role of strontium as doping agent in $LaMn_{0.5}Ni_{0.5}O_3$ for oxygen electro-catalysis. *Journal of Industrial and Engineering Chemistry*, **2020**, 85, 94-101.

4. Eom, C. J., Kuo, D. Y., Adamo, C., Moon, E. J., May, S. J., Crumlin, E. J.,& Suntivich, J. Tailoring manganese oxide with atomic precision to increase surface site availability for oxygen reduction catalysis. *Nature communications*,**2018**, 9(1), 1-7.

5. Yan, S., Xue, Y., Li, S., Shao, G., & Liu, Z. Enhanced bifunctional catalytic activity of manganese oxide/perovskite hierarchical core–shell materials by adjusting the interface for metal–air batteries. *ACS applied materials & interfaces*,**2019**, 11(29), 25870-25881.

6.González-Jiménez, I. N., Torres-Pardo, A., Rano, S., Laberty-Robert, C., Hernández-Garrido, J. C., López-Haro, M.,& Portehault, D. Multicationic $Sr_4Mn_3O_{10}$ mesostructures: molten salt synthesis, analytical electron microscopy study and reactivity. *Materials Horizons*, **2018**,5(3), 480-485.

7. Miao, H., Wang, Z., Wang, Q., Sun, S., Xue, Y., Wang, F., & Yuan, J. A new family of Mn-based perovskite ($La_{1-x}Y_xMnO_3$) with improved oxygen electrocatalytic activity for metal-air batteries. *Energy*, **2018**,154, 561-570.

8. Kotha, V., Karajagi, I., Ghosh, P. C., & Panchakarla, L. S. Potassium-Substituted $LaMnO_3$ as a Highly Active and Exceptionally Stable Electrocatalyst toward Bifunctional Oxygen Reduction and Oxygen Evolution Reactions. *ACS Applied Energy Materials*, **2022**

9. Fujiwara, Naoko, Tsukasa Nagai, Tsutomu Ioroi, Hajime Arai, and Zempachi Ogumi. "Bifunctional electrocatalysts of lanthanum-based perovskite oxide with Sb-doped SnO2 for oxygen reduction and evolution reactions." *Journal of Power Sources,* **2020,** 451,227736.

10. Zhao, Chunning, Meng Yu, Zhi Yang, Jieyu Liu, Shaohua Chen, Zhanglian Hong, Haijun Chen, and Weichao Wang. "Oxygen reduction reaction catalytic activity enhancement over mullite $SmMn_2O_5$ via interfacing with perovskite oxides." *Nano Energy,* **2018**, 51: 91-101.

11. Z. Lu, H. Zhou, B. Qian, S. Wang, Y. Zheng, L. Ge, H. Chen **.** Y and Fe co-doped $LaNiO_3$ perovskite as a novel bifunctional electrocatalyst for rechargeable zinc-air batteries." *International Journal of Hydrogen Energy,* **2023**, 48, no. 22, 8082-8092.

12. Li, T., Guo, W., & Shi, Q.. Nano-sized double perovskite oxide as bifunctional oxygen electrocatalysts. *International Journal of Electrochemical Science*, **2023**,*18*(5), 100103.

13. Ahmed, J., Ahamad, T., Alhokbany, N., Khan, M. M., Arunachalam, P., Amer, M. S., ... & Alshehri, S. M.. Reduced graphene oxide encapsulated perovskite-type lanthanum cobalt oxide nanoparticles for efficient electrolysis of water to oxygen reactions (OER/ORR). *Journal of Industrial and Engineering Chemistry*, **2023,***121*, 100-106.

14. L. Fengjiao, N. Mushtaq, T. Su, Y. Cui, J. Huang, M. Sun, M. Singh. "NCNT grafted perovskite oxide as an active bifunctional electrocatalyst for rechargeable zinc-air battery." *Materials Today Nano.* **2023**, 21, 100287.